

High Catalytic Activity and Chemoselectivity of Sub-nanometric Pd Clusters on Porous Nanorods of CeO₂ for Hydrogenation of Nitroarenes

Sai Zhang,[†] Chun-Ran Chang,[‡] Zheng-Qing Huang,[‡] Jing Li,[†] Zhemin Wu,[#] Yuanyuan Ma,[†] Zhiyun Zhang,[†] Yong Wang,[#] and Yongquan Qu^{*,†,§}

[†]Center for Applied Chemical Research, Frontier Institute of Science and Technology and State Key Laboratory for Mechanical Behavior of Materials, Xi'an Jiaotong University, Xi'an 710049, China

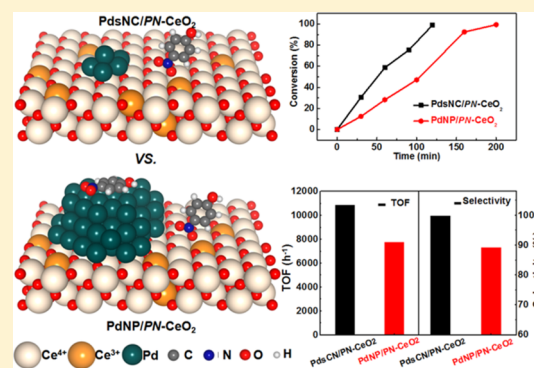
[‡]Institute of Industrial Catalysis, School of Chemical Engineering and Technology, Xi'an Jiaotong University, Xi'an 710049, China

[#]School of Material Science and Engineering, Centre of Electron Microscopy and State Key Laboratory of Silicon Materials, Zhejiang University, Hangzhou 310028, China

[§]MOE Key Laboratory for Nonequilibrium Synthesis and Modulation of Condensed Matter, Xi'an Jiaotong University, Xi'an 710049, China

Supporting Information

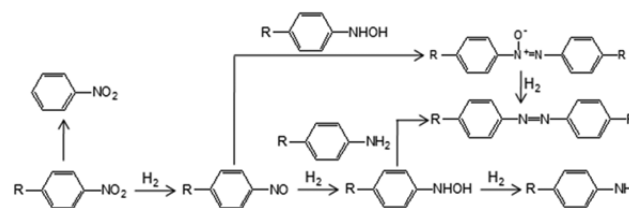
ABSTRACT: Sub-nanometric Pd clusters on porous nanorods of CeO₂ (PN-CeO₂) with a high Pd dispersion of 73.6% exhibit the highest catalytic activity and best chemoselectivity for hydrogenation of nitroarenes to date. For hydrogenation of 4-nitrophenol, the catalysts yield a TOF of ~44059 h⁻¹ and a chemoselectivity to 4-aminophenol of >99.9%. The superior catalytic performance can be attributed to a cooperative effect between the highly dispersed sub-nanometric Pd clusters for hydrogen activation and unique surface sites of PN-CeO₂ with a high concentration of oxygen vacancy for an energetically and geometrically preferential adsorption of nitroarenes via nitro group. The high concentration of surface defects of PN-CeO₂ and large Pd dispersion contribute to the enhanced catalytic activity for the hydrogenation reactions. The high chemoselectivity is mainly governed by the high Pd dispersion on the support. The catalysts also deliver high catalytic activity and selectivity for nitroaromatics with various reducible substituents into the corresponding aminoarenes.



1. INTRODUCTION

Anilines and their derivatives, especially with the functionalized groups, are key intermediates for the manufacture of pharmaceuticals, agrochemicals, dyes, and pigments.^{1,2} Non-catalytic reduction of the corresponding nitroarenes with stoichiometric reducing agents, such as sulfides, Fe, and Zn, is a widely used and effective process to produce the functionalized anilines in industry.³ However, these processes generate large amounts of waste acids and residues, which lead to serious environmental problems. In contrast, catalytic hydrogenation with the supported metal catalysts is an environmentally benign and highly efficient process for producing anilines.^{4,5} Nevertheless, the inevitable byproducts are also generated during the process as shown in Scheme 1.^{6–8} Nitroso- and azo-compounds as the major byproducts are unavoidable during the catalytic hydrogenation of nitro groups.⁹ The chemoselective hydrogenation of the substituted nitroarenes with the reducible functional groups (e.g., -OH, -Cl, -C=O, -C=C) is also a great challenge. Therefore, the development of more efficient and environmentally friendly

Scheme 1. Analysis of Possible Reaction Pathways for the Hydrogenation of Nitrobenzene Compounds



catalytic hydrogenation a process with high catalytic activity and chemoselectivity of nitroarenes is significant for both fundamental studies and industrial production.

Pt-group metals deliver high catalytic activity for hydrogenation of nitroarenes but poor selectivity.^{10–12} Despite the fact that selectivity can be improved with the aid of transition metal salts and additives, these metal salts and additives

Received: November 1, 2015

Published: February 1, 2016

decrease catalytic activity and raise new environmental problems.^{13,14} Au and Ag catalysts exhibit excellent chemoselectivity for hydrogenation of various nitroaromatics but poor catalytic activity due to their low ability for H₂ activation.^{7,15–17} Formation of alloys with Pt can increase the activity but sacrifice the chemoselectivity. Cobalt and iron oxides-based catalysts realize the highly chemoselective hydrogenation of nitroarenes.^{18–20} However, the reactions require more strict conditions: long reaction time (>12 h), high temperature (120 °C), and high H₂ pressure (5.0 MPa). Recently, Zhang's group reported single-atom and pseudo-single-atom Pt supported on FeO_x as the highly active and chemoselective catalysts for hydrogenation of variety of nitroaromatics.²¹ The performance is attributed to the presence of the positively charged Pt and absence of Pt–Pt metallic bonding, which favor the preferential adsorption of nitro groups. However, the chemoselectivity is generally reduced with the increase of catalytic activity.^{22,23} The chemoselective hydrogenation of nitrophenol, the most important nitro compound, is not reported in previous studies.^{4–11}

Previous studies have shown that nitro groups can be easily adsorbed on the basic or reducible supports.^{24,25} Ceria has been the subject of thorough investigations due to its unique surface properties with the dynamically reversible Ce³⁺/Ce⁴⁺ redox pair,^{26–28} which may forebode a strong interaction between CeO₂ surface and nitro groups. The single metal atoms or very small metal clusters anchored on the supports represent a new type of catalysts with the superior catalytic performance for various reactions.^{29–34} The specific locations and chemical bonding of the single metal atoms or clusters on supports lead to their unique electronic structures and strong interaction between metal and supports, which make them behave differently from their nanoparticle counterparts.^{35,36} The superior catalytic activity of Pt₁/FeO_x catalysts for CO oxidation and chemoselective hydrogenation of nitroaromatics can be attributed to the positively charged Pt on the reducible supports.^{21,37} The selective hydrogenation of unsaturated aldehydes by the single gold atoms on ZrO₂ support has been recognized as an Eley–Rideal mechanism rather than the Langmuir–Hinshelwood mechanism.³⁸ Besides, the unique electronic properties and particularity of scales for the single atom or clusters may introduce unique adsorption modes of reactants. The highly dispersed metals as isolated single atoms or very small clusters on the supports can decrease the coadsorption of two or more nitroarene molecules on metal greatly,³⁹ which may improve the selective hydrogenation of nitroarenes. Meanwhile, the highly dispersed metal catalysts have exhibited a good capability for H₂ activation for hydrogenation reactions.^{35,40–42}

Inspired by those facts, we report sub-nanometric Pd clusters supported on porous nanorods of CeO₂ (PN-CeO₂) with a high surface Ce³⁺ fraction and a large concentration of oxygen vacancy to serve as a novel catalyst (named as PdsNC/PN-CeO₂) with high catalytic activity and chemoselectivity for hydrogenation of various nitroarenes. For hydrogenation of 4-nitrophenol, the catalyst shows a high selectivity of >99.9% toward 4-aminophenol and a large turnover frequency (TOF) of ~44059 h⁻¹ based on exposed Pd atoms. Both experimental and theoretical results suggest that the superior catalytic activity and selectivity are originated from the cooperative effect between the highly dispersed Pd for H₂ dissociation and PN-CeO₂ for the highly preferential adsorption of nitroarenes.

2. RESULTS AND DISCUSSION

Photo-assisted Deposition of Sub-nanometric Pd Clusters on PN-CeO₂. The preparation of PN-CeO₂ involves a two-step hydrothermal method, as illustrated in our previous studies (Figure S1).^{43–47} Figure 1a shows the transmission

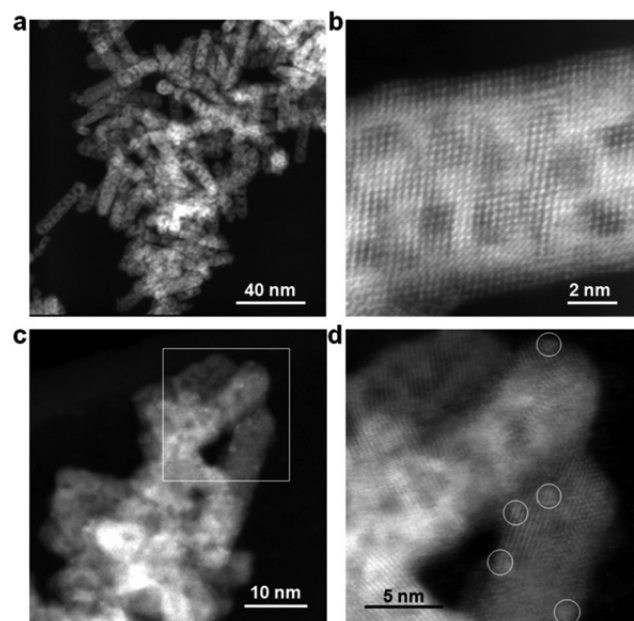


Figure 1. (a) Dark field TEM image and (b) high-resolution dark field TEM image of PN-CeO₂. (c, d) HAADF-STEM images of PdsNC/PN-CeO₂ catalysts.

electron microscopy (TEM) image of as-synthesized PN-CeO₂, which displays a rod-like morphology and a porous feature with a pore size of 2–4 nm. High-resolution dark-field TEM image (Figure 1b) further confirms the highly porous nature of PN-CeO₂. X-ray diffraction (XRD) spectrum (Figure S1b) indicates that as-prepared porous nanorods can be indexed to cubic fluorite structures. PdsNC/PN-CeO₂ is prepared through a photoassisted deposition method with Na₂PdCl₄ as precursor and methanol as sacrificial agent. Under light irradiation, the photogenerated electrons of PN-CeO₂ can reduce the adsorbed Pd ions. The collected solid is further treated in 5% H₂/Ar at 200 °C to completely reduce Pd species into Pd⁰. The actual Pd loading of 0.081 wt% on PN-CeO₂, determined by inductively coupled plasma optical emission spectroscopy (ICP-OES) analysis, is close to theoretical one of 0.1 wt%. No obvious Pd nanoparticles can be observed on the surface of PN-CeO₂ as shown in bright field TEM (Figure S2), suggesting a high Pd dispersion. CO chemisorption reveals a high Pd dispersion of 73.6%, which also shows very small amounts of internal Pd atoms and a very small size of Pd clusters. The PdsNC/PN-CeO₂ catalysts are further characterized by aberration-corrected high-angle annular dark field scanning transmission electron microscopy (HAADF-STEM, Figure 1c–d). On the basis of brightness variations, sub-nanometric clusters containing several to tens of Pd atoms with a size <0.9 nm are observed on the surface of PN-CeO₂. The presence of the Pd clusters in the PdsNC/PN-CeO₂ catalysts is further confirmed by a weak Pd signal in their energy-dispersive X-ray spectroscopy (EDS) spectrum (Figure S3).

Catalytic Activity of PdsNC/PN-CeO₂ for Hydrogenation of 4-Nitrophenol. Catalytic hydrogenation of 4-nitro-

phenol is used as a model reaction to illustrate the cooperative effects between $PN-CeO_2$ in richness of the surface-bound defects and the highly dispersed Pd to realize the highly catalytic selectivity to 4-aminophenol under mild conditions ($T = 80\text{ }^\circ\text{C}$ and $P(H_2) = 0.5\text{ MPa}$). Due to the high solubility of 4-nitrophenol in methanol, it is selected as the solvent for hydrogenation reactions. The optimized hydrogenation reactions of 4-nitrophenol are performed at $80\text{ }^\circ\text{C}$ under a H_2 pressure of 0.5 MPa (Table S1). When the $PN-CeO_2$ itself was used as the catalyst, no catalytic hydrogenation product was observed even within 600 min reaction (Table S1, Entries 15 and 16), demonstrating the inert nature of $PN-CeO_2$ for hydrogenation of 4-nitrophenol under the reaction conditions. In contrast, a near linear catalytic behavior of the $PdsNC/PN-CeO_2$ was shown in Figure 2a, where the conversion of 4-

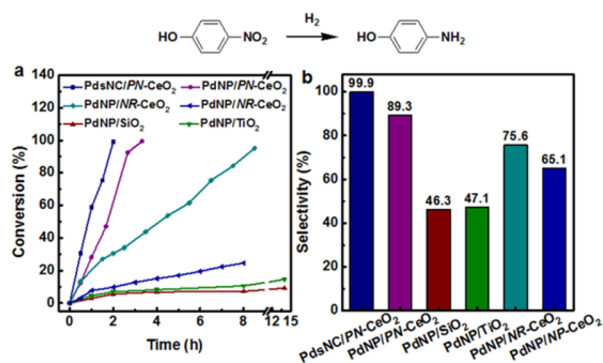


Figure 2. Catalytic activity and chemoselectivity of various Pd-catalysts for the hydrogenation of 4-nitrophenol. (a) The time course of conversion of 4-nitrophenol. (b) Chemoselectivity of 4-aminophenol catalyzed by various catalysts. Reaction condition: 0.5 mmol of 4-nitrophenol, 5 mg of catalysts, 4 mL of methanol, $80\text{ }^\circ\text{C}$, and $0.5\text{ MPa } H_2$.

nitrophenol was plotted as a function of reaction times. The calculated turnover frequency (TOF) based on each exposed Pd atom reaches 10900 h^{-1} (calculated for 30 min hydrogenation reaction), which is 1 or 2 orders of magnitude higher than those in literature under the similar conditions.^{4,24,48,49} More importantly, the chemoselectivity of 4-aminophenol can reach $>99.9\%$. The yield of byproducts is below the detection limitations of gas chromatography–mass spectrometry (GC-MS) and GC.

Catalytic activity and selectivity are contradictions in previous catalytic systems, in which the high catalytic activity is always at the expense of the catalytic chemoselectivity.^{50–52} For the $PdsNC/PN-CeO_2$, the complete conversion of 4-nitrophenol was realized within a shorter time of 1 h (Table S1, Entry 7) when H_2 pressure was increased to 2 MPa. When the reaction temperature was increased to $120\text{ }^\circ\text{C}$, the reaction time for the completed conversion of 4-nitrophenol was shortened into 30 min at a H_2 pressure of 0.5 MPa (Table S1, Entry 13). The calculated TOF of $PdsNC/PN-CeO_2$ for hydrogenation reaction at 10 min (Table S1, Entry 14) approaches 44059 h^{-1} , which is the highest value for hydrogenation of nitroarenes reported to date. Most impressively, the superior chemoselectivity of 4-nitrophenol into 4-aminophenol ($>99.9\%$) for both hydrogenation reactions (Table S1, Entry 7 and 13) is preserved, indicating the high catalytic performance of $PdsNC/PN-CeO_2$ for hydrogenation of nitroarenes.

To understand the benefits of highly dispersed Pd for the hydrogenation of 4-nitrophenol, the Pd nanoparticles/ $PN-CeO_2$ ($PdNP/PN-CeO_2$) catalysts with 0.1 wt% loading were also prepared by impregnation method and used for the hydrogenation of 4-nitrophenol under the same conditions. The Pd dispersion of the $PdNP/PN-CeO_2$ is 38.9%, which is determined by CO chemisorption. Some large Pd nanoparticles of 1.0–3.0 nm are observed on the $PN-CeO_2$ support (Figure S4a). The catalytic activity of the $PdNP/PN-CeO_2$ is lower than that of $PdsNC/PN-CeO_2$ catalysts (Figure 2a). The total conversion of 4-nitrophenol was realized for 3.5 h reaction and delivered a lower TOF of 7800 h^{-1} for $PdNP/PN-CeO_2$ (calculated for 30 min hydrogenation reaction and based on each exposed Pd atom). Moreover, the chemoselectivity of 4-aminophenol was decreased to 89.3% with a major byproduct of azo-compounds (Figure 2b).

Both sub-nanometric Pd clusters and PdNPs exhibit much higher activity if compared with previous reports,^{4,24,39,40} revealing that $PN-CeO_2$ plays very important roles for the hydrogenation of nitroarenes. To examine this assumption, PdNPs on SiO_2 (Figure S4d) and TiO_2 (Figure S4e) supports with 0.1 wt% Pd loading were prepared by impregnation method, and their catalytic activity was evaluated at the identical reaction conditions. Both $PdNP/SiO_2$ and $PdNP/TiO_2$ catalysts delivered very poor catalytic activity (Figure 2a). The conversions of 4-nitrophenol were only 5.6% and 6.98% at 2 h for the $PdNP/SiO_2$ and $PdNP/TiO_2$ catalysts, respectively. Meanwhile, large amounts of byproducts, such as 4-nitrosophenol and azoxy, were produced for the hydrogenation reactions catalyzed by $PdNP/SiO_2$ and $PdNP/TiO_2$. The chemoselectivity of 4-nitrophenol into 4-aminophenol is very poor for $PdNP/SiO_2$ (46.3%) and $PdNP/TiO_2$ (47.1%) when the conversion of 4-nitrophenol is below 15% (Figure 2b).

To further examine the important roles of $PN-CeO_2$ for the hydrogenation of nitroarenes, nonporous nanorods of CeO_2 ($NR-CeO_2$) and nanoparticles of CeO_2 ($NP-CeO_2$) were also employed as supports for Pd nanoparticles (0.1 wt%) by impregnation method (Figures S4b and S4c). For $PdNP/NR-CeO_2$ catalysts, the conversion of 4-nitrophenol was 30.5% after 2 h reaction, which was 2.6 and 4.3 times lower than those of the $PdNP/PN-CeO_2$ and $PdsNC/PN-CeO_2$ catalysts, respectively. Meanwhile, the chemoselectivity of 4-nitrophenol into 4-aminophenol is only 75.6% for the $PdNP/NR-CeO_2$ catalysts with 95.1% conversion of 4-nitrophenol. This selectivity is much lower than that of $PdNP/PN-CeO_2$ at the similar reactant conversion. The even lower catalytic activity and poorer selectivity for the $PdNP/NP-CeO_2$ catalysts were observed (Figure 2b). Compared to the catalytic performance of the $PdNP/PN-CeO_2$ catalysts, the results indicate that $PN-CeO_2$ as support benefits the enhanced catalytic activity and improved chemoselectivity of the hydrogenation of 4-nitrophenol. It can be attributed to the abundant surface defects of $PN-CeO_2$, which will be discussed later.

Mechanism of Catalytic Behavior of $PdsNC/PN-CeO_2$. The control experiments indicate that both the highly dispersed Pd and $PN-CeO_2$ support contribute to very high catalytic activity and superior chemoselectivity for hydrogenation of 4-nitrophenol. To understand such unique catalytic behaviors of $PdsNC/PN-CeO_2$, investigations on the adsorption model of reactants on the $PdsNC/PN-CeO_2$ and $PdNP/PN-CeO_2$ catalysts become important.^{25,53–55} Nitro group, a well-known strong electron-withdrawing group, has a strong interaction with the electron-rich sites of various heterogeneous

catalysts. Both $PN\text{-CeO}_2$ with a high richness of surface oxygen vacancy as strong Lewis-basic sites⁴⁴ and metallic Pd can serve as the adsorbed sites for nitro groups. Hence, DFT calculations of the adsorption energy of 4-nitrophenol on various possible sites of catalysts, including $PN\text{-CeO}_2$ support and Pd nanocatalysts of various sizes, were performed to study the interaction between nitro group and catalysts.

As shown in Figure S5, 4-nitrophenol molecule can be weakly adsorbed on the ideal (111) crystal face of CeO_2 , which is optimized on the top of Ce atom with an adsorption energy of -0.22 eV. $PN\text{-CeO}_2$ possesses the characteristic to display a very high capacity for oxygen storage ($900 \mu\text{mol O}_2/\text{g}$) due to the high Ce^{3+} surface fraction and large concentration of oxygen vacancy.⁴⁴ Hence, the reduced CeO_2 support is created by introducing surface defects of oxygen vacancy and Ce^{3+} species. The calculated adsorption energy of -1.45 eV for 4-nitrophenol on the surface defect of the reduced CeO_2 is 6.6 times higher than that on the ideal CeO_2 surface. Such a strong interaction between the surface defects of $PN\text{-CeO}_2$ and nitro group makes it effortless to form a specific structure, in which 4-nitrophenol molecule lies perpendicularly to the reduced CeO_2 surface via two oxygen atoms of nitro group interacting with three Ce atoms nearby an oxygen vacancy (Figure 3). The

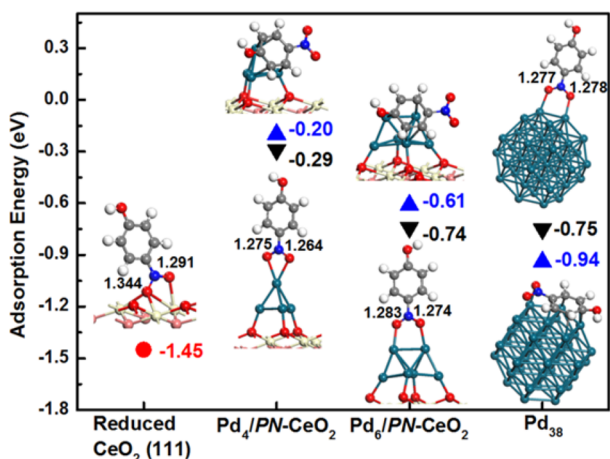


Figure 3. Summary of adsorption models of 4-nitrophenol on Pd nanocatalysts of various sizes and $PN\text{-CeO}_2$ support. Adsorption energies (eV) and bond length (Å) are labeled in the figure. Note: $PN\text{-CeO}_2$ was not considered for large Pd_{38} in order to save computational resource.

strong interaction is further confirmed by the Fourier transform infrared (FTIR) spectra of 4-nitrophenol molecules on various supports, as shown in Figure 4. Compared with the FTIR spectrum of $PN\text{-CeO}_2$, three characteristic peaks at 1210, 1460, and 1540 cm^{-1} are presented after adsorption of 4-nitrophenol, which can be assigned to the stretching vibration of C–OH, framework vibration of benzene, and asymmetrical stretch of NO_2 , respectively (Figure 4a). In contrast, no obvious characteristic peaks of 4-nitrophenol on SiO_2 (Figure 4b) and TiO_2 (Figure 4c) supports before and after adsorption are observed. FTIR analysis of the adsorption of 4-nitrophenol on $NR\text{-CeO}_2$ (Figure S6a) or $NP\text{-CeO}_2$ (Figure S6b) shows much weaker characteristic peaks of the adsorbed molecules on both supports, indicating the poor interaction between 4-nitrophenol and $NR\text{-CeO}_2/NP\text{-CeO}_2$. Combined with adsorption energy of 4-nitrophenol on reduced and ideal CeO_2 surface (Figures 3 and S5), the dramatic difference in the adsorption profiles of 4-

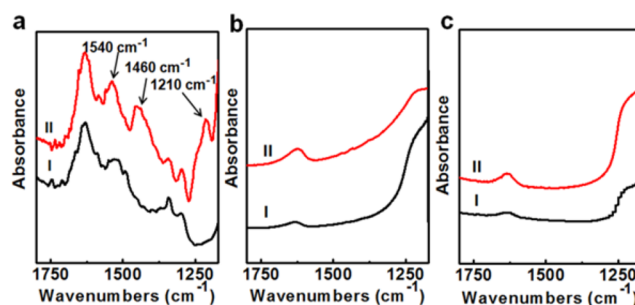


Figure 4. FTIR spectra of (a) $PN\text{-CeO}_2$, (b) SiO_2 , and (c) TiO_2 supports before (I) and after (II) adsorption of 4-nitrophenol, respectively.

nitrophenol on three ceria can be attributed to their different surface defects, in which the surface Ce^{3+} fraction (30.8%) of $PN\text{-CeO}_2$ is much higher than those of $NR\text{-CeO}_2$ (15.7%) and $NP\text{-CeO}_2$ (9.3%) obtained from the XPS analysis (Figure S7). The FTIR results further confirm the strong interaction between 4-nitrophenol and $PN\text{-CeO}_2$, which can be attributed to its richness of surface defects. Thus, the utilization of $PN\text{-CeO}_2$ as the support of metal nanocatalysts can contribute to the catalytic performance of Pd significantly.

To study the adsorption of 4-nitrophenol on Pd clusters, small clusters (Pd_4 and Pd_6) supported on $PN\text{-CeO}_2$ and large cluster Pd_{38} (~ 1 nm) without support are used as computational models (Figure S8). The 4-nitrophenol molecule may bond with Pd clusters via the oxygen atoms in nitro group and/or via the aromatic ring.⁵⁶ When 4-nitrophenol binds with Pd via the oxygen atoms, it anchors at the top of the clusters with the molecular plane almost perpendicular to the CeO_2 surface. The adsorption energy of 4-nitrophenol in this mode is -0.29 eV on Pd_4/CeO_2 and -0.74 eV on Pd_6/CeO_2 , which are 5.00 and 1.96 times lower (in absolute value) than that of 4-nitrophenol on reduced CeO_2 (111), -1.45 eV (Figure 3). Meanwhile, owing to the size limit of small Pd clusters and steric hindrance, the adsorption energies of 4-nitrophenol on Pd_4/CeO_2 and Pd_6/CeO_2 via aromatic ring are -0.20 and -0.61 eV (Figure 3), respectively, indicating the adsorption via aromatic ring on small clusters is less stable than that via the oxygen atoms in nitro group. To extend the Pd clusters to a large size, the adsorption of 4-nitrophenol on Pd_{38} was also evaluated. As shown in Figure 3, in comparison with small clusters, 4-nitrophenol preferentially binds with Pd_{38} via aromatic ring with an adsorption energy of -0.94 eV, which is more stable than the adsorption via oxygen atoms in nitro group on Pd_{38} (-0.75 eV), Pd_6 (-0.74 eV), and Pd_4 clusters (-0.29 eV).

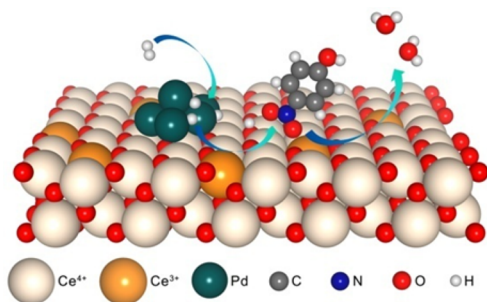
Therefore, 4-nitrophenol molecules are preferentially adsorbed on the $PN\text{-CeO}_2$ rather than the Pd cluster species for the $\text{Pd}_{38}/PN\text{-CeO}_2$ catalyst. Such a large adsorption energy (-1.45 eV) on reduced CeO_2 surface can benefit the complete conversion of 4-nitrophenol into 4-aminophenol with a pretty low selectivity to nitroso-compounds. With the increased size of Pd cluster, the adsorption energy and adsorption sites of 4-nitrophenol on Pd catalysts are increased simultaneously, which results in the adsorbed 4-nitrophenol not only on $PN\text{-CeO}_2$ but also on Pd nanoparticles during hydrogenation reaction. Once multiple 4-nitrophenol molecules are adsorbed on large Pd nanoparticles, the diffusion of 4-nitrophenol and subsequent coupling reactions between nitroarenes will occur readily, leading to a decreased chemoselectivity to 4-aminophenol.

Conclusively, the large difference in adsorption energy of 4-nitrophenol on PdsNC, PdNP and PN-CeO₂ can significantly affect the catalytic activity and selectivity of the PdsNC/PN-CeO₂ and PdNP/PN-CeO₂.

Besides the dependence of Pd dispersion-adsorption energy of 4-nitrophenol (DFT calculations), the steric hindrance of coadsorption of multiple 4-nitrophenol molecules on Pd catalysts of various sizes also may affect the chemoselectivity. When the size of Pd cluster is large enough, it can provide sufficient sites for the coadsorption of two or more nitroarenes. In this case, the catalytic coupling into the byproducts of azo-compounds can happen. In contrast, the very small Pd clusters or even monodispersed Pd atoms are not accessible for multiple reactants at the same time due to the large steric hindrance. Therefore, the high selectivity of 4-nitrophenol catalyzed by PdsNC/PN-CeO₂ is expected and indeed realized.

Both experimental and theoretical results demonstrate an obvious cooperative effect between the highly dispersed Pd for H₂ dissociation and PN-CeO₂ for the preferential adsorption of 4-nitrophenol. Based on the calculated adsorption models (Figure 3), a mechanism for high catalytic activity and chemoselectivity can be proposed, as shown in Scheme 2.

Scheme 2. Proposed Catalytic Process for Hydrogenation of Nitroarenes Catalyzed by the PdsNC/PN-CeO₂ Catalysts



PN-CeO₂ with a high surface concentration of oxygen vacancy serves as the adsorbed sites for 4-nitrophenol. When Pd catalysts are highly dispersed on the PN-CeO₂ support, 4-nitrophenol molecules can be preferentially adsorbed on PN-CeO₂. The Pd serves as the catalysts for H₂ dissociation and produces the active hydrogen species, which can be used to reduce the adsorbed reactants nearby. After the complete hydrogenation, 4-aminophenol can be desorbed from PN-CeO₂ support. The high catalytic selectivity can be realized. When the large PdNPs are used as catalysts, nitro group of reactants can be adsorbed on both Pd nanoparticles and PN-CeO₂ support. Hydrogen activation and absorption of multiple reactants on lowly dispersed Pd nanocatalysts allow the reduction of nitro into amine and subsequent coupling reactions between nitroarenes, leading to the poor chemoselectivity.

The high catalytic activity of PdsNC/PN-CeO₂ can be also revealed from DFT calculations. When 4-nitrophenol interacts with the reduced CeO₂ surface, the lengths of two N–O bonds can be extended into 1.291 and 1.344 Å, respectively, compared with the intrinsic length 1.245 Å of 4-nitrophenol (Figure S5a). In contrast, two N–O bonds are only lengthened to ~1.28 Å or even shorter for 4-nitrophenol on Pd₆ or Pd₃₈ cluster. This differentiation indicates that the greatly weakened N–O bonds for the reactants adsorbed on PN-CeO₂ benefit the hydrogenation reactions, revealing higher catalytic activity of PdsNC/PN-CeO₂.

Effects of Surface Defects of PN-CeO₂ and Pd Dispersion on the Activity and Selectivity of 4-Nitrophenol Hydrogenation.

Both experimental results and theoretical calculations indicate that the Pd dispersion and concentration of surface defects of PN-CeO₂ are critical for the catalytic activity and selectivity for the hydrogenation of 4-nitrophenol. In order to further examine the proposed catalytic mechanism, as-synthesized catalysts were calcined at 300 and 500 °C for 8 h after photoassisted deposition of Pd on PN-CeO₂ supports and reduced by 5% H₂/Ar at 200 °C for 2 h to completely reduce Pd species into Pd⁰. In this case, the metal dispersion and concentration of surface defects can be regulated by the calcination temperatures, while the morphology of the catalysts is well preserved (Figure S9). The obtained catalysts were named as PdsNC/PN-CeO₂-300 and PdsNC/PN-CeO₂-500, respectively. Derived from their XPS profiles (Figure S7), the surface Ce³⁺ fractions of PdsNC/PN-CeO₂-300 and PdsNC/PN-CeO₂-500 are decreased from 27.4% of as-synthesized PdsNC/PN-CeO₂ catalysts to 17.5% and 13.8%, respectively. Generally, the presence of Ce³⁺ is a result of oxygen vacancy and the concentration of oxygen vacancy of CeO₂ is greatly associated with the surface Ce³⁺ fractions.^{57,58} The surface defects of various catalysts are further examined by Raman spectroscopy, in which the concentration of oxygen vacancy can be indexed by the ratio (A_{600}/A_{460}) of the integrated peak areas at 600 cm⁻¹ (oxygen vacancy) and 460 cm⁻¹ (vibrational mode of CeO₂ fluorite structure).⁵⁹ As shown in Figure S10, the decreased values of A_{600}/A_{460} for PdsNC/PN-CeO₂ (0.149), PdsNC/PN-CeO₂-300 (0.1), and PdsNC/PN-CeO₂-500 (0.087) further reveal the richness of surface defects for three catalysts in the order of PdsNC/PN-CeO₂ > PdsNC/PN-CeO₂-300 > PdsNC/PN-CeO₂-500, which is consistent with XPS measurements (Figure 5a). Thus, the concentration of surface defects of the catalysts is decreased with the increased calcination temperatures.

Meanwhile, the Pd dispersion of 72.1% for the PdsNC/PN-CeO₂-300 catalysts is similar to that of the PdsCN/PN-CeO₂ (73.6%) determined by CO adsorption. In contrast, the Pd dispersion of the PdsCN/PN-CeO₂-500 is decreased to 42.5% due to the surface diffusion and aggregation of Pd species induced by the high calcination temperature. Thus, the current catalytic systems provide an unambiguous platform to investigate the effects of the controllable metal dispersion and surface defects of PN-CeO₂ on the hydrogenation reactions due to the same morphology, crystal surfaces, synthetic approach, and the similar accessibility of reactants.

The catalytic profiles of hydrogenation 4-nitrophenol as a function of reaction times on various Pd/PN-CeO₂ catalysts under the identical reaction conditions are presented in Figure 5b. Under the used conditions, the PdsNC/PN-CeO₂ catalysts with the highest Pd dispersion (73.6%) and the largest surface Ce³⁺ fraction of 27.4% delivered the best catalytic activity. It took 120 min for the PdsNC/PN-CeO₂ to reach near complete conversion of 4-nitrophenol, which was 30, 80, and 90 min shorter than those for the PdsNC/PN-CeO₂-300, PdNP/PN-CeO₂, and PdsNC/PN-CeO₂-500 catalysts, respectively (Figure 5b).

Catalytic activity of various catalysts is further characterized by TOFs (calculations are based on the exposed Pd atoms) as functions of the surface Ce³⁺ fraction and Pd dispersion (Figure 5 and Table S2). As shown in Figure 5c, with the similar Pd dispersion, the PdsNC/PN-CeO₂ with the higher surface Ce³⁺ fraction (27.4%) shows much higher catalytic activity (TOF =

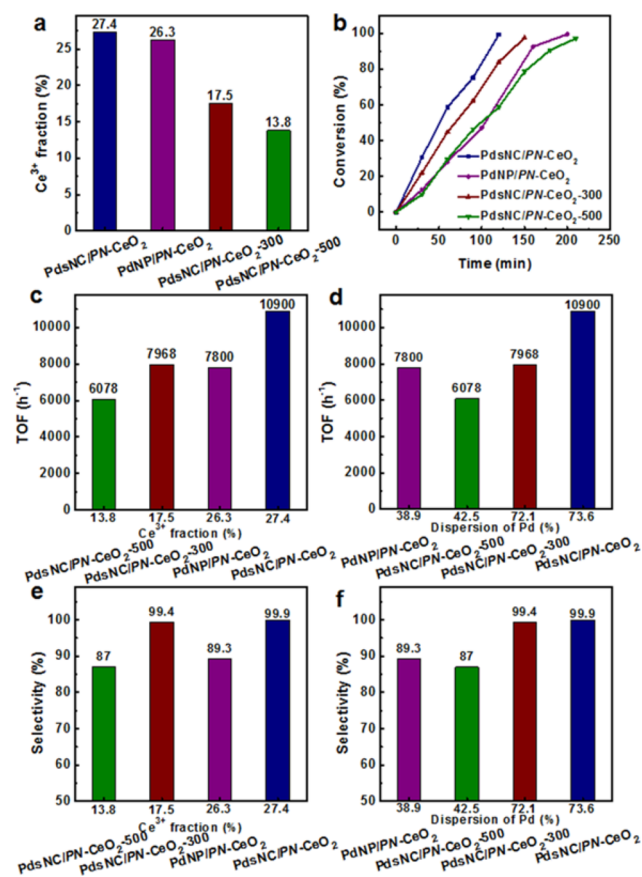


Figure 5. Effects of the surface Ce^{3+} fractions and Pd dispersion on their catalytic performance of 4-nitrophenol hydrogenation. (a) Surface Ce^{3+} fractions for various Pd nanocatalysts on PN-CeO_2 . (b) Catalytic profiles of various catalysts as a function of time for 4-nitrophenol hydrogenation. (c) Plot of the surface Ce^{3+} fractions of various catalysts and their TOFs. (d) Plot of the Pd dispersion of various catalysts and their TOFs. (e) Plot of the surface Ce^{3+} fractions of various catalysts and their chemoselectivity. (f) Plot of the Pd dispersion of various catalysts and their chemoselectivity. TOFs are calculated for hydrogenation reactions at 30 min as shown in (b) and based on each exposed Pd atom (determined by CO chemisorption). Reaction condition: 0.5 mmol of 4-nitrophenol, 5 mg of catalysts, 4 mL of methanol, 80 °C, and 0.5 MPa H_2 .

10900 h^{-1}), which is 1.37 times higher than that of the $\text{PdsNC/PN-CeO}_2\text{-300}$ ($\text{TOF} = 7968 \text{ h}^{-1}$) with a low surface Ce^{3+} fraction of 17.5%. Despite the PdNP/PN-CeO_2 having a much lower Pd dispersion of 38.9%, it has a high surface Ce^{3+} fraction of 26.3%, it still delivers catalytic activity ($\text{TOF} = 7800 \text{ h}^{-1}$) similar to that of the $\text{PdsNC/PN-CeO}_2\text{-300}$ and much better than that of $\text{PdsNC/PN-CeO}_2\text{-500}$ catalysts ($\text{TOF} = 6078 \text{ h}^{-1}$). For the $\text{PdsNC/PN-CeO}_2\text{-300}$ and $\text{PdsNC/PN-CeO}_2\text{-500}$, the decreased surface Ce^{3+} fraction leads to a decreased surface concentration of oxygen vacancy serving as the adsorbed sites for 4-nitrophenol. Therefore, less amounts of 4-nitrophenol molecules can be adsorbed on the surface adsorption sites, which results in the decreased catalytic activity, obviously. Figure 5d shows the catalytic activity of the four catalysts as a function of the Pd dispersion. Generally, the higher dispersion of Pd results in the higher values of TOF, except for the PdNP/PN-CeO_2 catalysts. The relative high catalytic activity of the PdNP/PN-CeO_2 can be attributed to the high surface Ce^{3+} fractions as described above. The results reveal that the catalysts with a higher surface Ce^{3+} fraction provide more active sites for

the adsorption of 4-nitrophenol and then deliver higher catalytic activity. Meanwhile, the high Pd dispersion represents the high Pd dispersion nature for hydrogen adsorption and accelerates the hydrogenation reaction subsequently.^{30,33} The results are also consistent with the simulation results reflected by the lengthened bond length of N–O bonds after the adsorption on the surface defects of the PN-CeO_2 support (Figure 3).

Figure 5e,f shows the chemoselectivity of 4-nitrophenol hydrogenation toward 4-aminophenol as functions of the surface Ce^{3+} fraction and Pd dispersion. As shown in theoretical calculations on the adsorption energy of 4-nitrophenol on sub-nanometric Pd clusters, nanoparticles and PN-CeO_2 support (Figure 3), and FTIR profiles (Figure 4), because of their energy and geometry, 4-nitrophenol molecules preferentially adsorbed on the surface defects of PN-CeO_2 via nitro group. With the decrease of Pd dispersion, the coadsorption of 4-nitrophenol on Pd and PN-CeO_2 became possible, leading to the decreased chemoselectivity. Hence, the PdNP/PN-CeO_2 and $\text{PdsNC/PN-CeO}_2\text{-500}$ with low Pd dispersion (below 43%) deliver poor chemoselectivity (Figure 5f). Despite the reduced surface Ce^{3+} fraction and decreased catalytic activity, the $\text{PdsNC/PN-CeO}_2\text{-300}$ maintains a very high chemoselectivity of 99.4% (Figure 5e). It can be attributed to the high Pd dispersion of 72.1% for the $\text{PdsNC/PN-CeO}_2\text{-300}$, which benefits the preferential adsorption of 4-nitrophenol on the surface defects of PN-CeO_2 , refrains from the multiple adsorption of reactants on Pd nanoparticles, and avoids the possibility to generate byproducts. Obviously, the chemoselectivity is slightly affected by the surface defects of PN-CeO_2 , but is indeed governed by the metal Pd dispersion.

Summarizing from Figure 5, the large concentration of the surface defects of PN-CeO_2 and high Pd dispersion can significantly contribute to the high catalytic activity for the 4-nitrophenol hydrogenation reaction. The high chemoselectivity is mainly dependent on the Pd dispersion, which induces an energetically and geometrically preferential adsorption on the surface defective sites of PN-CeO_2 .

Catalytic Stability. The catalytic stability is also a very important criterion to evaluate the catalysts. The PdsNC/PN-CeO_2 can be easily recycled by centrifugation and reused up to six cycles. To evaluate catalytic stability of the PdsNC/PN-CeO_2 , the 4-nitrophenol hydrogenation reaction was performed at 1.5 h. As shown in Figure 6, the conversion of 4-nitrophenol

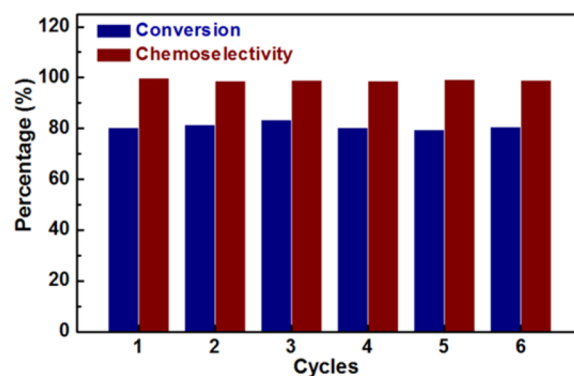
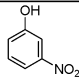
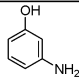
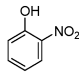
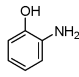
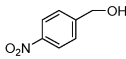
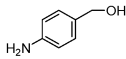
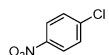
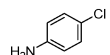
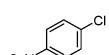
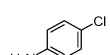
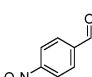
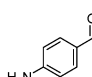
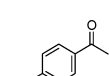
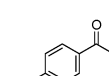
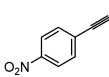
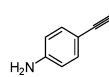


Figure 6. Catalytic stability and selectivity of PdsNC/PN-CeO_2 catalysts at 1.5 h reaction time. Reaction condition: 0.5 mmol of 4-nitrophenol, 5 mg of catalysts, 4 mL of methanol, 80 °C, and 0.5 MPa H_2 .

remains for the six cycles. Especially, the chemoselectivity of the PdsNC/PN-CeO₂ is also preserved (>99.9%) for the 4-nitrophenol hydrogenation reaction toward 4-aminophenol during the six cycles. The unchanged morphological features of the PdsNC/PN-CeO₂ catalysts (Figure S11) with their undegraded catalytic activity and chemoselectivity further demonstrate the excellent catalytic stability of the catalysts.

Scope of Hydrogenation of Nitroarenes. The reaction protocol was further extended to various substituted nitroarenes including various reducible groups to verify the scope, activity, and chemoselectivity of hydrogenation reactions catalyzed by the PdsNC/PN-CeO₂ (Table 1). For 2 h

Table 1. Hydrogenation of Various Substituted Nitroarenes Catalyzed by PdsNC/PN-CeO₂ Catalysts^a

Entry	Substrate	Product	Time (h)	Con. (%)	Sel. (%)
1			2	93.3	>99.9
2			2	98.3	99.0
3			4	98.3	>99.9
4			1	70	95.8
5			1.5	>99.9	92.8
6			2	>99.9	98.0
7			2	>99.9	>99.9
8			3	>99.9	98.0

^aReaction condition: 0.5 mmol substrate in 4 mL methanol, 5 mg PdsNC/PN-CeO₂ catalysts, 0.5 MPa H₂, and 80 °C. The conversion and selectivity were determined by GC-MS and GC with *m*-xylene as internal standard.

hydrogenation reactions, the chemoselectivity of 2-nitrophenol and 3-nitrophenol reached 99.9% (93.3% conversion, Entry 1) and 99.0% (98.3% conversion, Entry 2), respectively. Meanwhile, 98.3% of conversion and >99.9% of selectivity were also obtained for the *p*-nitrobenzyl alcohol as substrate (Entry 3). The catalytic activity and selectivity of nitroarenes with the reducible substituents were also evaluated for PdsNC/PN-CeO₂. A high percentage of aniline impurity is common and unavoidable for the hydrogenation of 4-chloronitrobenzene, an important intermediate for the manufacture of 4-chloroaniline. When the PdsNC/PN-CeO₂ was used as the catalysts, a high selectivity of 95.8% and 92.8% of 4-chloroaniline can be obtained with the conversion of 70% and >99.9%, respectively (Entries 4 and 5). The PdsNC/PN-CeO₂ catalysts also exhibited good chemoselective hydrogenation of nitro group in the presence of a broad spectrum of substituents containing -CHO, -C(CH₃)=O, and -CN functional group. The

selectivity to functionalized anilines was greater than 98% when the conversion of nitroarenes reach >99.9% (Entries 6–8).

3. CONCLUSIONS

In conclusion, the subnano Pd clusters on PN-CeO₂ with the high activity and chemoselectivity for hydrogenation of nitroarenes have been successfully synthesized by a photo-assisted deposition method. The superior catalytic performance can be attributed to the synergistic effect between the highly dispersed sub-nanometric Pd cluster and unique surface properties of PN-CeO₂ support. For highly dispersed Pd catalysts, a preferential adsorption of nitro group at the oxygen vacancy of PN-CeO₂ and hydrogen activation on Pd resulted in high catalytic activity and selectivity. When PdNP/PN-CeO₂ is used as catalyst, nitro groups of reactants can be adsorbed on both PdNPs and PN-CeO₂ support. Hydrogen activation and adsorption of multiple reactants on the PdNPs allow the reduction of nitro groups into amine and the subsequent coupling reactions between amine, leading to a poor chemoselectivity. The strong interaction between nitro and PN-CeO₂ can effectively weaken the N–O bonds of nitro and enhance the catalytic activity of Pd/PN-CeO₂ for hydrogenation reaction. Such unique cooperative effects between the highly dispersed metals and supports for the preferential adsorption of reactants may benefit the design of novel catalysts with high catalytic activity and chemoselectivity for many important reactions.

4. EXPERIMENTAL SECTION

All chemicals (AR grade) were used as received. Water with a resistivity of 18.2 MΩ·cm was used for all experiments. All glassware was thoroughly washed by aqua regia (a volume ratio of 1:3 of concentrated nitric acid and hydrochloric acid) to avoid any possible contamination.

Synthesis of PN-CeO₂. PN-CeO₂ was synthesized by our previously reported method,⁴⁴ which involved a two-step hydrothermal method. Briefly, a mixture of 1.367 g of Ce(NO₃)₃·6H₂O and 19.2 g of NaOH in 70 mL of water was treated with hydrothermal process at 100 °C for 24 h in a Pyrex bottle to obtain nonporous Ce(OH)₃/CeO₂ nanorods. Subsequently, the PN-CeO₂ was synthesized by hydrothermal treatment on nonporous Ce(OH)₃/CeO₂ nanorods in a stainless steel autoclave at 160 °C temperatures for 12 h.

Synthesis of NR-CeO₂. Ce(NO₃)₃·6H₂O (1.736 g) and NaOH (19.2 g) were dissolved in 10 and 70 mL of MQ water, respectively. After aging for 30 min, the mixture was transferred into a stainless steel autoclave for hydrothermal treatment at 100 °C for 24 h. The solid products were collected by centrifugation, washed with copious MQ water, and dried at 60 °C.

Synthesis of NP-CeO₂. The nanoparticles of ceria were obtained by direct calcination of Ce(NO₃)₃·6H₂O in air at 500 °C for 2 h.

Synthesis of PdsNC/PN-CeO₂ Catalysts. PdsNC/PN-CeO₂ catalysts with a 0.083 wt% metal loading were prepared with a photoassisted deposition method, in which Na₂PdCl₄ was used as Pd precursor and methanol served as the sacrifice agent. Typically, 300 mg of PN-CeO₂ was suspended in a mixed solvent of 36 mL of H₂O and 4 mL of methanol at room temperature. After the desired amount of Na₂PdCl₄ was added, the solution was degassed with Ar for 30 min and then irradiated for 3 h under a Xe lamp. The catalysts were centrifuged off, washed with water, and dried at 60 °C. Finally, the PdsNC/PN-CeO₂ catalysts were treated in 5% H₂/Ar at 200 °C to completely reduce Pd species into Pd⁰.

Synthesis of PdNP/PN-CeO₂, PdNP/SiO₂, PdNP/TiO₂, PdNP/NR-CeO₂, and PdNP/NP-CeO₂ Catalysts. Pd nanoparticle catalysts supported on PN-CeO₂, SiO₂, TiO₂, NR-CeO₂, and NP-CeO₂ were prepared by a wet impregnation method. Briefly, the supports were

dispersed in an ethanol solution with proper amount of Na_2PdCl_4 at room temperature. After the mixture was continuously stirred at room temperature for 2 h, ethanol was evaporated at $80\text{ }^\circ\text{C}$ and the solids were dried at $60\text{ }^\circ\text{C}$ for 12 h. Finally, the Pd nanoparticles catalysts were further treated in $5\% \text{H}_2/\text{Ar}$ at $200\text{ }^\circ\text{C}$ to reduce Pd species into Pd^0 .

Characterization of Catalysts. The phase evolution of as-synthesized nanostructures was monitored by powder X-ray diffraction (XRD). The XRD patterns with diffraction intensity versus 2θ were recorded in a Shimadzu X-ray diffractometer (Model 6000) using $\text{Cu K}\alpha$ radiation. Transmission electron microscopy (TEM) studies were conducted on a Hitachi HT-7700 transmission electron microscope with an accelerating voltage of 120 kV. HAADF-STEM and EDX analysis were conducted on a FEI Titan G² 80-200 ChemiSTEM instrument. The dispersion of Pd was derived from CO chemisorption by using pulses of a gas mixture containing 10% CO in He at room temperature. A given amount of CO ($50\text{ }\mu\text{L}$) was introduced in a pulse per 5 min until the intensity of the peak reached a constant value. Fourier transform infrared (FTIR) analysis of the samples was taken on a Thermo Scientific Nicolet 6700 Fourier transform infrared spectroscopy. All of the samples were mixed with KBr and pressed into a thin plate for measurement. The Pd content was determined by inductively coupled plasma optical emission spectroscopy (ICP-OES) analysis (Agilent 7500ce).

Catalytic Hydrogenation of Nitroarenes. The hydrogenation of nitroarenes was carried out in a stainless steel autoclave equipped with pressure control system. For a typical catalytic reaction, 0.5 mmol nitroarenes and 5 mg catalysts were mixed in 4 mL of methanol. The reactions were performed in the autoclave charged with 0.5 MPa of hydrogen at $80\text{ }^\circ\text{C}$. The products were analyzed by gas chromatography–mass spectrometer (GC-MS) and GC with m-xylene as internal standard. TOFs are calculated by eqs 1 and 2 and based on each exposed Pd atom:

$$\text{TOF} = \frac{n_0 C}{t n_{\text{cat}}} \quad (1)$$

$$n_{\text{cat}} = \frac{m_{\text{cat}} w}{M_{\text{Pd}}} \text{Dis}_{\text{Pd}} \quad (2)$$

where n_0 is the initial molar of substrate, C is the conversion of substrates at the reaction of t , n_{cat} is the molar of exposed Pd atom, w is the mass fraction of Pd in catalysts, M_{Pd} is molar mass of Pd, and Dis_{Pd} is the dispersion of Pd for catalysts.

Computational Method. All spin-polarized DFT calculations were carried out using the Vienna *ab initio* simulation package (VASP).^{60–62} The electron exchange–correlation potential was treated by the generalized gradient approximation (GGA) in the form of Perdew–Burke–Ernzerhof (PBE) functional.⁶³ The wave functions were expanded in a plane wave basis with an energy cutoff of 400 eV, using a projector augmented wave (PAW) method. The DFT + U methodology^{64,65} was used to treat the on-site Coulomb and exchange interactions of the strongly localized Ce 4f electrons. An effective $U = 4.5\text{ eV}$ value was chosen as previous studies suggested.⁶⁶

Brillouin zone integration was sampled with the $6 \times 6 \times 6$ and $3 \times 3 \times 1$ Monkhorst–Pack mesh k -points for bulk and surface calculations, respectively.⁶⁷ The optimized lattice parameter of the bulk CeO_2 crystal, $a = 5.468\text{ \AA}$, is in good agreement with experimental value of 5.411 \AA .⁶⁸ The $\text{CeO}_2(111)$ surface was represented by a six-layer slab with $p(3 \times 3)$ supercell and the bottom three layers of the slab were constrained to their optimal bulk positions. The neighboring slabs were separated by a vacuum region of 15 \AA in the direction perpendicular to the surface. When the adsorbates were perpendicularly anchored on the surface, the vacuum space was increased to 20 \AA to avoid image interaction. For calculations on Pd clusters, a unit cell of $20 \times 20 \times 25\text{ \AA}$ is presented to prevent interactions between neighboring unit cells. For 4-nitrophenol, a unit cell of $20 \times 20 \times 20\text{ \AA}$ is used. The Brillouin zone integration was sampled with $1 \times 1 \times 1$ Monkhorst–Pack mesh k -points for calculations on Pd clusters and 4-nitrophenol. The structures were considered relaxed when all forces on

each ion were smaller than 0.02 eV/\AA , and the convergence criterion for the energy was 10^{-5} eV .

The adsorption energies, E_{ads} , are calculated by using the following equation:

$$E_{\text{ads}} = E_{\text{adsorbate+surface}} - (E_{\text{adsorbate}} + E_{\text{surface}})$$

where $E_{\text{adsorbate+surface}}$ is the total energy of surface covered with adsorbates, $E_{\text{adsorbate}}$ is the energy of adsorbate, and E_{surface} is the energy of clean surface. With this definition, a negative value of E_{ads} means a release of energy or a stable adsorption on the surface.

■ ASSOCIATED CONTENT

Supporting Information

The Supporting Information is available free of charge on the ACS Publications website at DOI: 10.1021/jacs.5b11413.

More detailed information regarding structural characterization of PN-CeO_2 , EDS spectrum of $\text{Pd}_4\text{NC/PN-CeO}_2$ catalysts, TEM images of $\text{Pd}_4\text{NC/PN-CeO}_2$, PdNP/PN-CeO_2 , PdNP/NR-CeO_2 , PdNP/NP-CeO_2 , PdNP/SiO_2 and PdNP/TiO_2 , the optimized structure and bond distances (\AA) of 4-nitrophenol, the adsorption model of 4-nitrophenol on the ideal (111) crystal face of CeO_2 , the FTIR spectra of NR-CeO_2 and NP-CeO_2 supports before and after absorption of 4-nitrophenol, the calculation model of $\text{Pd}_4/\text{PN-CeO}_2$, $\text{Pd}_6/\text{PN-CeO}_2$ and Pd_{38} nanoparticle, TEM images of $\text{Pd}_4\text{NC/PN-CeO}_2$ -300 and $\text{Pd}_4\text{NC/PN-CeO}_2$ -500 catalysts, XPS spectrum and Raman spectra of various catalysts, TEM image of the $\text{Pd}_4\text{NC/PN-CeO}_2$ catalysts after 6 cycle of catalytic reactions and the optimization of reaction condition for hydrogenation of 4-nitrophenol (PDF)

■ AUTHOR INFORMATION

Corresponding Author

* yongquan@mail.xjtu.edu.cn

Notes

The authors declare no competing financial interest.

■ ACKNOWLEDGMENTS

We acknowledge the financial support from a NSFC Grant 21201138, 21401148, the National 1000-Plan program, and NSFC Grant 51390474. This work was also partially funded by the Ministry of Science and Technology of China through a 973-program under Grant 2012CB619401 and by the Fundamental Research Funds for the Central Universities under Grant xjj2013102 and xjj2013043. Authors thank the State Key Laboratory for Mechanical Behavior of Materials (Dr. Yuanbin Qin) and Frontier Institute of Science and Technology for TEM technical support. We thank Prof. Jun Li at Tsinghua University for help in getting access to the software of VASP. All calculations were performed by using supercomputers at the Shanghai Supercomputing Center and the Shen-Zhen Cloud Computing Center.

■ REFERENCES

- (1) Müller, T. E.; Hultsch, K. C.; Yus, M.; Foubelo, F.; Tada, M. *Chem. Rev.* **2008**, *108*, 3795–3892.
- (2) Hartwig, J. F. *Nature* **2008**, *455*, 314–322.
- (3) Junge, K.; Wendt, B.; Shaikh, N.; Beller, M. *Chem. Commun.* **2010**, *46*, 1769–1771.
- (4) Tamura, M.; Kon, K.; Satsuma, A.; Shimizu, K. I. *ACS Catal.* **2012**, *2*, 1904–1909.

- (5) Tomkins, P.; Gebauer-Henke, E.; Leitner, W.; Müller, T. E. *ACS Catal.* **2015**, *5*, 203–209.
- (6) He, D.; Jiao, X.; Jiang, P.; Wang, J.; Xu, B. Q. *Green Chem.* **2012**, *14*, 111–116.
- (7) Corma, A.; Serna, P. *Science* **2006**, *313*, 332–334.
- (8) Vilé, G.; Almora-Barrios, N.; López, N.; Pérez-Ramírez, J. *ACS Catal.* **2015**, *5*, 3767–3778.
- (9) Liu, X.; Li, H. Q.; Ye, S.; Liu, Y. M.; He, H. Y.; Cao, Y. *Angew. Chem., Int. Ed.* **2014**, *53*, 7624–7628.
- (10) Nie, R.; Wang, J.; Wang, L.; Qin, Y.; Chen, P.; Hou, Z. *Carbon* **2012**, *50*, 586–596.
- (11) Kataoka, S.; Takeuchi, Y.; Harada, A.; Takagi, T.; Takenaka, Y.; Fukaya, N.; Yasuda, H.; Ohmori, T.; Endo, A. *Appl. Catal., A* **2012**, *427*, 119–124.
- (12) Gu, J.; Zhang, Z.; Hu, P.; Ding, L.; Xue, N.; Peng, L.; Guo, X.; Lin, M.; Ding, W. *ACS Catal.* **2015**, *5*, 6893–6901.
- (13) Corma, A.; Serna, P.; Concepción, P.; Calvino, J. J. *J. Am. Chem. Soc.* **2008**, *130*, 8748–8753.
- (14) Makosch, M.; Lin, W. I.; Bumbálek, V.; Sá, J.; Medlin, J. W.; Hungerbühler, K.; van Bokhoven, J. A. *ACS Catal.* **2012**, *2*, 2079–2081.
- (15) He, D.; Shi, H.; Wu, Y.; Xu, B. Q. *Green Chem.* **2007**, *9*, 849–851.
- (16) Chen, Y.; Wang, C.; Liu, H.; Qiu, J.; Bao, X. *Chem. Commun.* **2005**, 5298–5300.
- (17) Wang, F.; Liu, J.; Xu, X. *Chem. Commun.* **2008**, 2040–2042.
- (18) Jagadeesh, R. V.; Surkus, A. E.; Junge, H.; Pohl, M.-M.; Radnik, J.; Rabeah, J.; Huan, H.; Schünemann, V.; Brückner, A.; Beller, M. *Science* **2013**, *342*, 1073–1076.
- (19) Jagadeesh, R. V.; Banerjee, D.; Arockiam, P. B.; Junge, H.; Junge, K.; Pohl, M.-M.; Radnik, J.; Brückner, A.; Beller, M. *Green Chem.* **2015**, *17*, 898–902.
- (20) Jagadeesh, R. V.; Stemmler, T.; Surkus, A.-E.; Junge, H.; Junge, K.; Beller, M. *Nat. Protoc.* **2015**, *10*, 548–557.
- (21) Wei, H.; Liu, X.; Wang, A.; Zhang, L.; Qiao, B.; Yang, X.; Huang, Y.; Miao, S.; Liu, J.; Zhang, T. *Nat. Commun.* **2014**, *5*, 5634.
- (22) Guo, H.; Yan, X.; Zhi, Y.; Li, Z.; Wu, C.; Zhao, C.; Wang, J.; Yu, Z.; Ding, Y.; He, W.; Li, Y. *Nano Res.* **2015**, *8*, 1365–1372.
- (23) Shukla, A.; Singha, R. K.; Sasaki, T.; Bal, R. *Green Chem.* **2015**, *17*, 785–790.
- (24) Corma, A.; Serna, P.; García, H. *J. Am. Chem. Soc.* **2007**, *129*, 6358–6359.
- (25) Boronat, M.; Concepción, P.; Corma, A.; González, S.; Illas, F.; Serna, P. *J. Am. Chem. Soc.* **2007**, *129*, 16230–16237.
- (26) Vivier, L.; Duprez, D. *ChemSusChem* **2010**, *3*, 654–678.
- (27) Aydin, C.; Lu, J.; Browning, N. D.; Gates, B. C. *Angew. Chem., Int. Ed.* **2012**, *51*, 5929–5034.
- (28) Yang, M.; Li, S.; Wang, Y.; Herron, J. A.; Xu, Y.; Allard, L. F.; Lee, S.; Huang, J.; Mavrikakis, M.; Flytzani-Stephanopoulos, M. *Science* **2014**, *346*, 1498–1501.
- (29) Liang, S.; Hao, C.; Shi, Y. *ChemCatChem* **2015**, *7*, 2559–2567.
- (30) Huang, Z.; Gu, X.; Cao, Q.; Hu, P.; Hao, J.; Li, J.; Tang, X. *Angew. Chem., Int. Ed.* **2012**, *51*, 4198–4203.
- (31) Zhang, X.; Guo, J.; Guan, P.; Liu, C.; Huang, H.; Xue, F.; Dong, X.; Pennycook, S. J.; Chisholm, M. F. *Nat. Commun.* **2013**, *4*, 1924.
- (32) Xing, J.; Chen, J. F.; Li, Y. H.; Yuan, W. T.; Zhou, Y.; Zheng, L. R.; Wang, H. F.; Hu, P.; Wang, Y.; Zhao, H. J.; Yang, H. G. *Chem. - Eur. J.* **2014**, *20*, 2138–2144.
- (33) Kistler, J. D.; Chotigkrai, N.; Xu, P.; Enderle, B.; Praserthdam, P.; Chen, C. Y.; Browning, N. D.; Gates, B. C. *Angew. Chem., Int. Ed.* **2014**, *53*, 8904–8907.
- (34) Okrut, A.; Runnebaum, R. C.; Ouyang, X.; Lu, J.; Aydin, C.; Hwang, S.-J.; Zhang, S.; Olatunji-Ojo, O. A.; Durkin, K. A.; Dixon, D. A. *Nat. Nanotechnol.* **2014**, *9*, 459–465.
- (35) Yang, X.-F.; Wang, A.; Qiao, B.; Li, J.; Liu, J.; Zhang, T. *Acc. Chem. Res.* **2013**, *46*, 1740–1748.
- (36) Hackett, S. F.; Brydson, R. M.; Gass, M. H.; Harvey, I.; Newman, A. D.; Wilson, K.; Lee, A. F. *Angew. Chem., Int. Ed.* **2007**, *46*, 8593–8596.
- (37) Qiao, B.; Wang, A.; Yang, X.; Allard, L. F.; Jiang, Z.; Cui, Y.; Liu, J.; Li, J.; Zhang, T. *Nat. Chem.* **2011**, *3*, 634.
- (38) Wang, C.-M.; Fan, K.-N.; Liu, Z.-P. *J. Catal.* **2009**, *266*, 343–350.
- (39) Zhang, S.; Nguyen, L.; Liang, J. X.; Shan, J.; Liu, J.; Frenkel, A. I.; Patlolla, A.; Huang, W.; Li, J.; Tao, F. *Nat. Commun.* **2015**, *6*, 7938.
- (40) Li, Z. Y.; Yuan, Z.; Li, X. N.; Zhao, Y. X.; He, S. G. *J. Am. Chem. Soc.* **2014**, *136*, 14307–14313.
- (41) Li, F.; Li, Y.; Zeng, X. C.; Chen, Z. *ACS Catal.* **2015**, *5*, 544–552.
- (42) Lin, J.; Wang, A.; Qiao, B.; Liu, X.; Yang, X.; Wang, X.; Liang, J.; Li, J.; Liu, J.; Zhang, T. *J. Am. Chem. Soc.* **2013**, *135*, 15314–15317.
- (43) Zhang, S.; Li, J.; Gao, W.; Qu, Y. *Nanoscale* **2015**, *7*, 3016–3021.
- (44) Li, J.; Zhang, Z.; Tian, Z.; Zhou, X.; Zheng, Z.; Ma, Y.; Qu, Y. *J. Mater. Chem. A* **2014**, *2*, 16459–16466.
- (45) Tian, Z.; Li, J.; Zhang, Z.; Gao, W.; Zhou, X.; Qu, Y. *Biomaterials* **2015**, *59*, 116–124.
- (46) Zhang, S.; Chang, C.-R.; Huang, Z.-Q.; Ma, Y.; Gao, W.; Li, J.; Qu, Y. *ACS Catal.* **2015**, *5*, 6481–6488.
- (47) Zhang, Z.; Li, J.; Gao, W.; Ma, Y.; Qu, Y. *J. Mater. Chem. A* **2015**, *3*, 18074–18082.
- (48) Beier, M. J.; Andanson, J. M.; Baiker, A. *ACS Catal.* **2012**, *2*, 2587–2595.
- (49) Sharma, U.; Kumar, N.; Verma, P. K.; Kumar, V.; Singh, B. *Green Chem.* **2012**, *14*, 2289–2293.
- (50) Wu, B.; Huang, H.; Yang, J.; Zheng, N.; Fu, G. *Angew. Chem., Int. Ed.* **2012**, *51*, 3440–3443.
- (51) Kahsar, K. R.; Schwartz, D. K.; Medlin, J. W. *J. Am. Chem. Soc.* **2014**, *136*, 520–526.
- (52) Shimizu, K.-i.; Miyamoto, Y.; Kawasaki, T.; Tanji, T.; Tai, Y.; Satsuma, A. *J. Phys. Chem. C* **2009**, *113*, 17803–17811.
- (53) Baker, L. R.; Kennedy, G.; Van Spronsen, M.; Hervier, A.; Cai, X.; Chen, S.; Wang, L. W.; Somorjai, G. A. *J. Am. Chem. Soc.* **2012**, *134*, 14208–14216.
- (54) Lim, K. H.; Mohammad, A. B.; Yudanov, I. V.; Neyman, K. M.; Bron, M.; Claus, P.; Rösch, N. *J. Phys. Chem. C* **2009**, *113*, 13231–13240.
- (55) Kennedy, G.; Baker, L. R.; Somorjai, G. A. *Angew. Chem., Int. Ed.* **2014**, *53*, 3405–3408.
- (56) Hensley, A. J.; Wang, Y.; McEwen, J. S. *Surf. Sci.* **2014**, *630*, 244–253.
- (57) Esch, F.; Fabris, S.; Zhou, L.; Montini, T.; Africh, C.; Fornasiero, P.; Comelli, G.; Rosei, R. *Science* **2005**, *309*, 752–755.
- (58) Dutta, P.; Pal, S.; Seehra, M. S.; Shi, Y.; Eyring, E. M.; Ernst, R. D. *Chem. Mater.* **2006**, *18*, 5144–5146.
- (59) Wang, Y.; Wang, F.; Song, Q.; Xin, Q.; Xu, S.; Xu, J. *J. Am. Chem. Soc.* **2013**, *135*, 1506–1515.
- (60) Kresse, G.; Hafner, J. *Phys. Rev. B: Condens. Matter Mater. Phys.* **1994**, *49*, 14251–14269.
- (61) Kresse, G.; Furthmüller, J. *Comput. Mater. Sci.* **1996**, *6*, 15–50.
- (62) Kresse, G.; Furthmüller, J. *Phys. Rev. B: Condens. Matter Mater. Phys.* **1996**, *54*, 11169–11186.
- (63) Perdew, J. P.; Burke, K.; Ernzerhof, M. *Phys. Rev. Lett.* **1996**, *77*, 3865–3868.
- (64) Anisimov, V. I.; Zaanen, J.; Andersen, O. K. *Phys. Rev. B: Condens. Matter Mater. Phys.* **1991**, *44*, 943–954.
- (65) Dudarev, S. L.; Botton, G. A.; Savrasov, S. Y.; Humphreys, C. J.; Sutton, A. P. *Phys. Rev. B: Condens. Matter Mater. Phys.* **1998**, *57*, 1505–1509.
- (66) Fabris, S.; Vicario, G.; Balducci, G.; de Gironcoli, S.; Baroni, S. *J. Phys. Chem. B* **2005**, *109*, 22860–22867.
- (67) Monkhorst, H. J.; Pack, J. D. *Phys. Rev. B* **1976**, *13*, 5188–5192.
- (68) Kümmeler, E. A.; Heger, G. J. *Solid State Chem.* **1999**, *147*, 485–500.